Chapter 4
Rosette Tensile Fracture

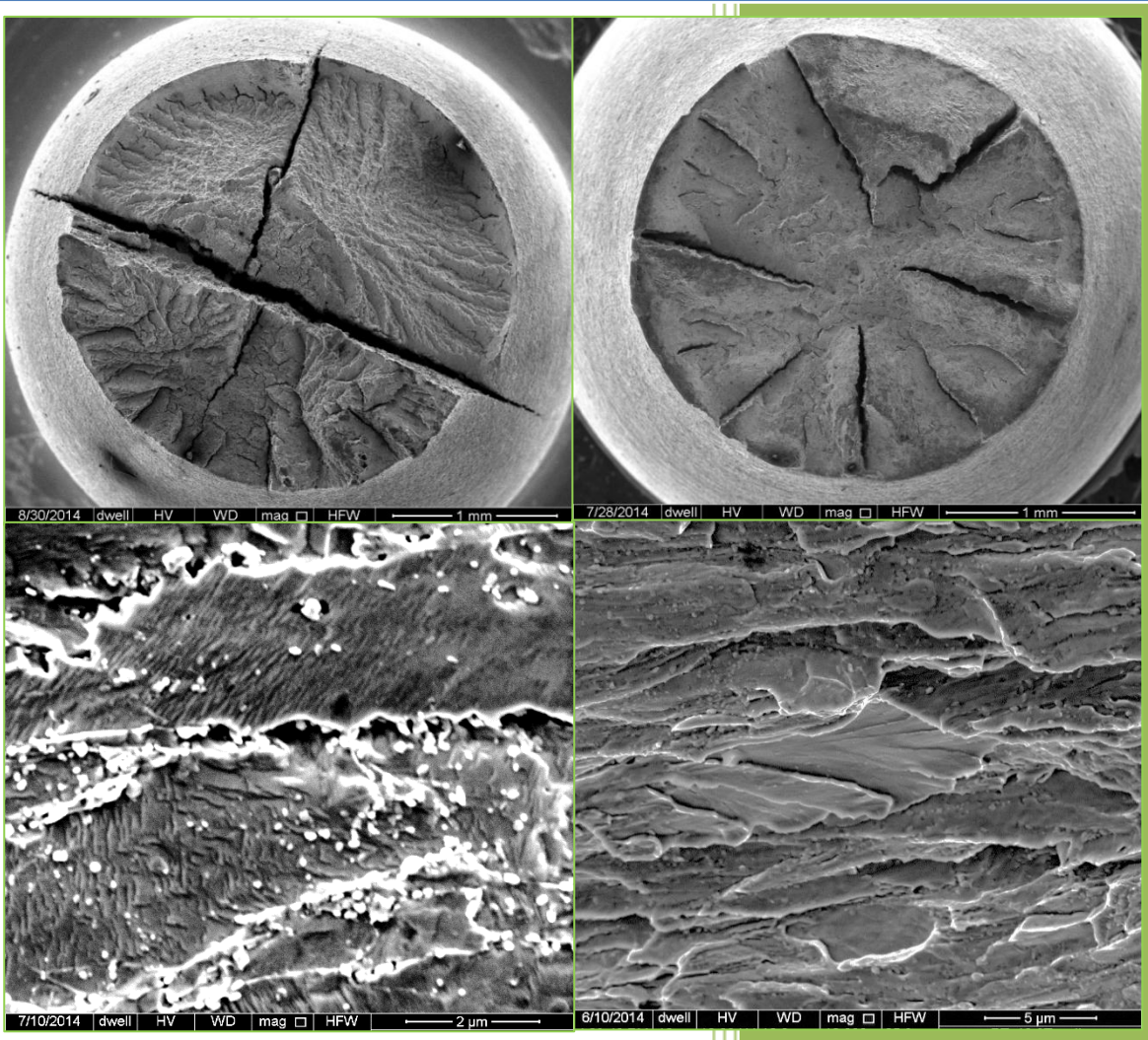

4.1 Introduction

It is seen in the previous chapter that this modified 9Cr–1Mo steel in normalized and tempered condition exhibits typical rosette fracture with central fibrous zone, radial cracking at different angular intervals and very fine shear lip zone. This chapter deals with detailed investigation of this typical rosette fracture. Role of different variables such as temperature, microstructure, strain rate, texture and plastic constraint on rosette fracture is studied. Radial cracks are observed on the fracture surface at different angular intervals. These cracks propagated longitudinally and are mostly associated with prior austenite grain boundaries and lath boundaries. Rosette fracture is found to be affected by test temperature, microstructure (in particular the number density, size and distribution of carbide precipitates along the prior austenite grain boundaries/lath boundaries) and the plastic constraint, however, there is no effect of texture. The process of rosette fracture is found to be associated with void formation at carbide particles, lying at the prior austenite grain boundaries and lath boundaries and their rapid linkage along the boundaries oriented along the stress axis.

4.2 Effect of Temperature on Rosette Fracture

Variation of 0.2 % offset yield strength (YS) and ultimate tensile strength (UTS) with temperature is shown in Fig. 4.1. Both YS as well as UTS decreases with increase in temperature and there is relatively faster drop in strength above 50 °C. The rate of fall in UTS with temperature is relatively higher than that in the YS. Variation of total and uniform elongation is shown in Fig. 4.1. There is no significant variation in total elongation (TE) with temperature, however, the uniform elongation (UE) decreases with rise in temperature.

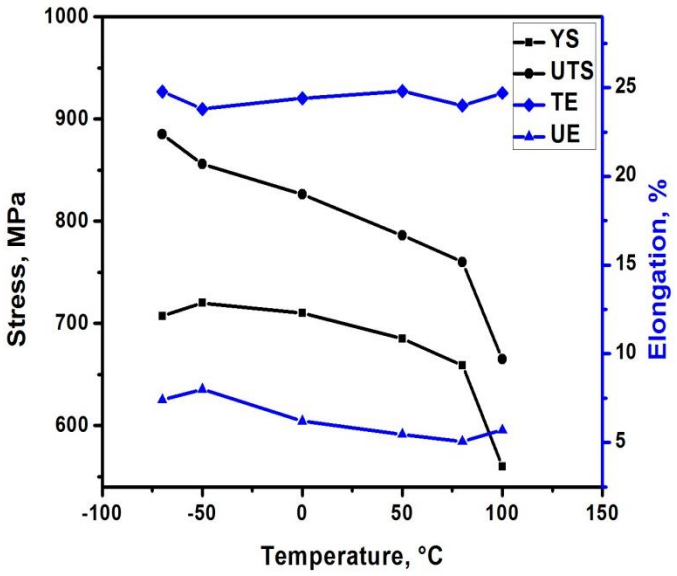

Fig. 4.1 Effect of temperature on strength and elongation in normalized and tempered (N_1+T) condition.

Effect of test temperature on fracture behavior over the temperature range -70 °C to 100 °C is shown in Fig. 4.2. There is normal cup and cone fracture with apparent fibrous zone in the central region and double shear lip zone in peripheral region of the specimen tested at 100 °C (Fig. 4.2a). As the test temperature decreases from 100 °C to room temperature (RT), the usual cup and cone fracture is observed to disappear, the fibrous zone in central region is reduced in size and becomes smoother and there is radial cracking in the plane of fracture at different angular intervals. The radial cracks are associated with longitudinal splitting along the tensile stress axis. At the test temperature of 80 °C radial cracks were observed to originate slightly away from the fibrous zone and propagate almost to periphery of the fracture surface (Fig. 4.2b). Further lowering of test temperature from 80 °C to 25 °C shifts the origin of radial cracking towards the center of loading axis and the fibrous zone decreases also the shear lip zone decreases with lowering of temperature.

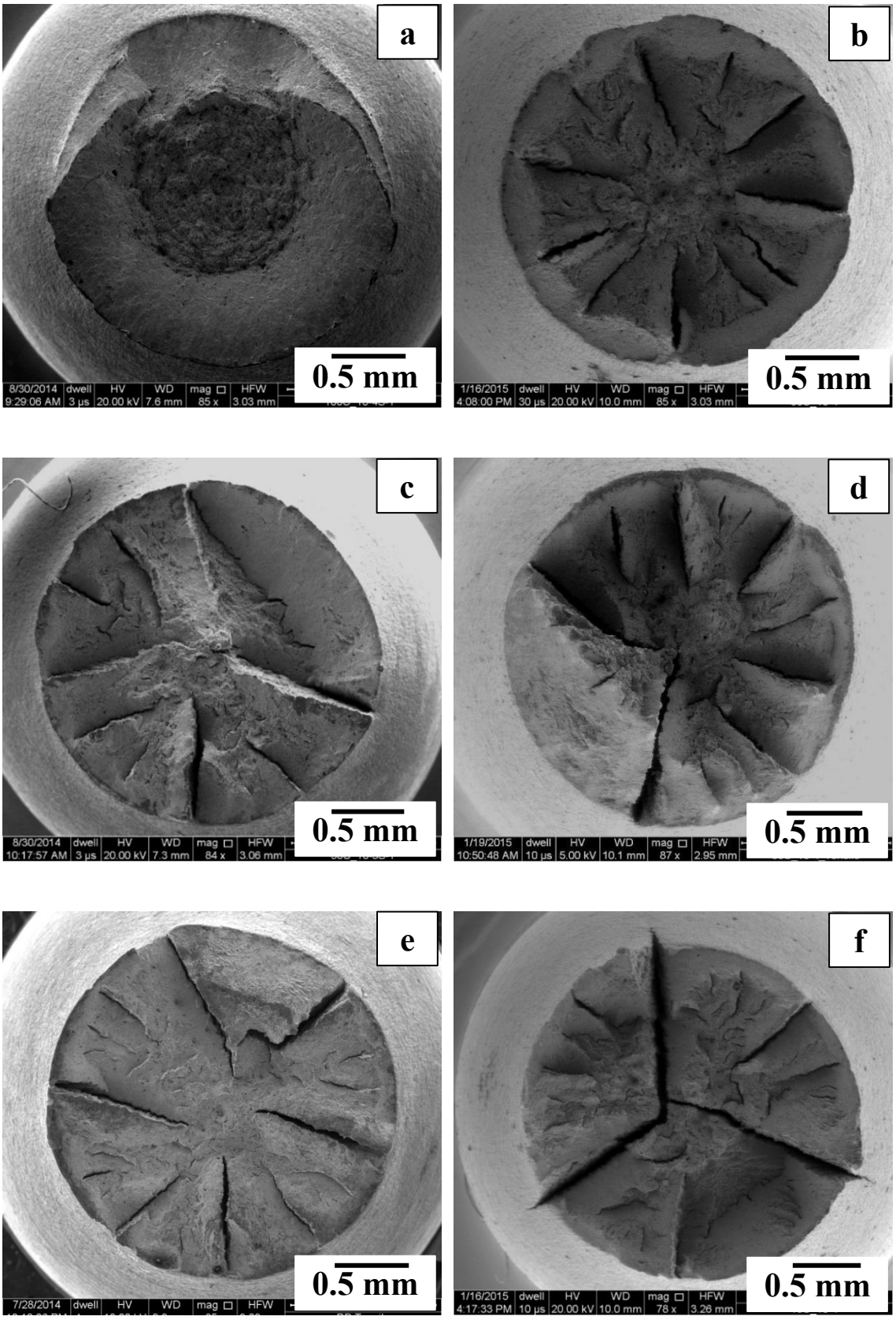
a
0.5 mm
b
0.5 mm
c
0.5 mm
d
0.5 mm
e
0.5 mm
f
0.5 mm

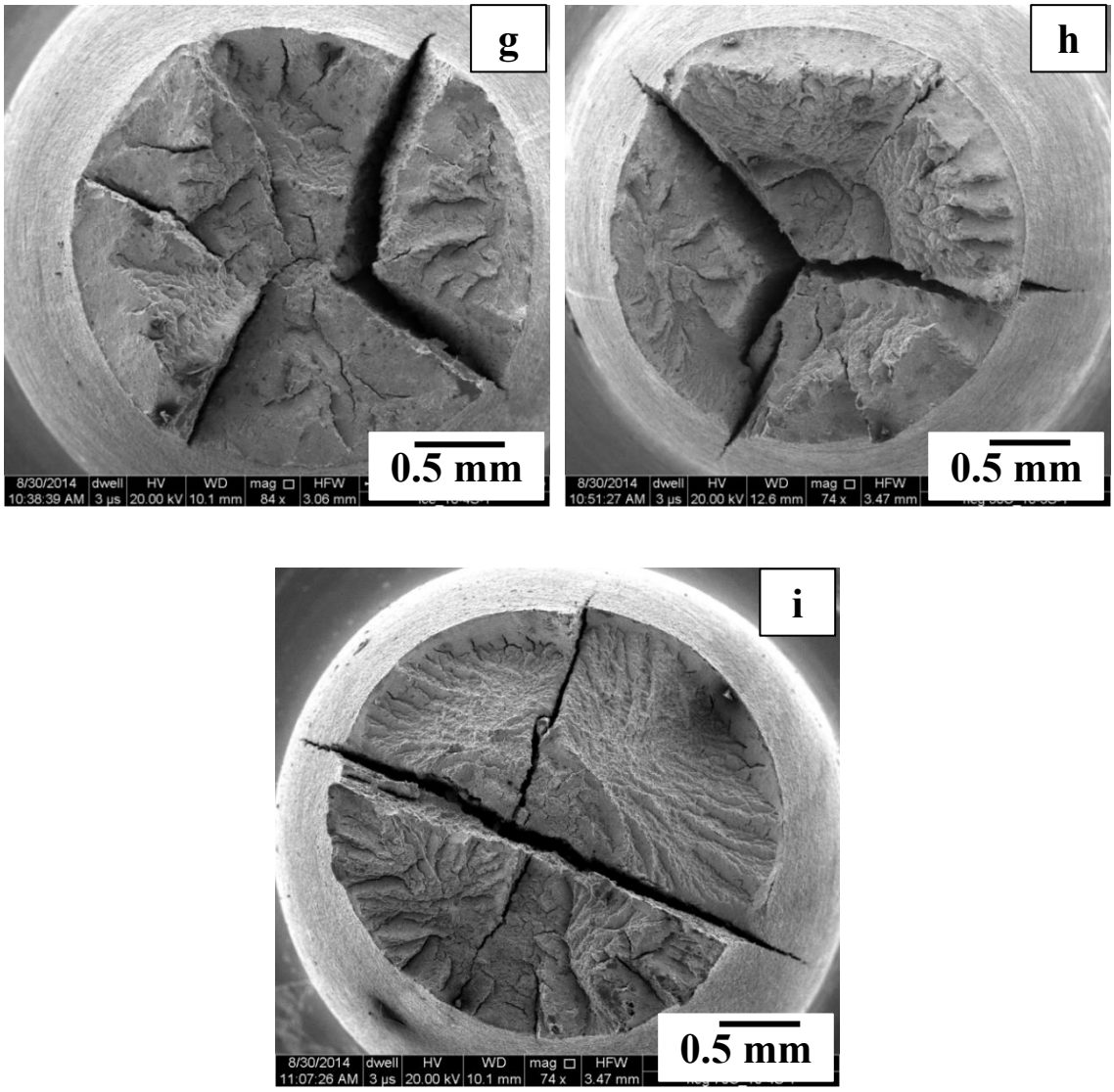

Fig. 4.2. Overall fracture surfaces showing the effect of test temperature in the N_1+T condition, on the nature of fracture: (a) 100 °C, (b) 80 °C, (c) 50 °C, (d) 30°C, (e) RT, (f) 13 °C, (g) 0 °C, (h) -50 °C and (i) -70 °C.

It is also important to mention that the severity of longitudinal splitting in terms of depth, length, and width of the radial cracks increases with decrease in temperature; however, the number of radial cracks is reduced. With further fall in temperature, from 13 °C to -70 °C, the depth of radial cracks is significantly increased. Thus, the severity of longitudinal cracking increases with decrease in temperature. The number of longitudinal splitting (along the stress axis) decreases and the length of longitudinal splitting increases with decrease in test temperature.

The morphology of fibrous zone of the fractured specimens tested at different temperatures of 100 °C, 50 °C, 0 °C & -70 °C is shown in Fig. 4.3. It may be seen that fibrous zone of the specimen tested even at 100 °C exhibiting cup and cone fracture shows mixed features of small facets and fine dimples (Fig. 4.3a).

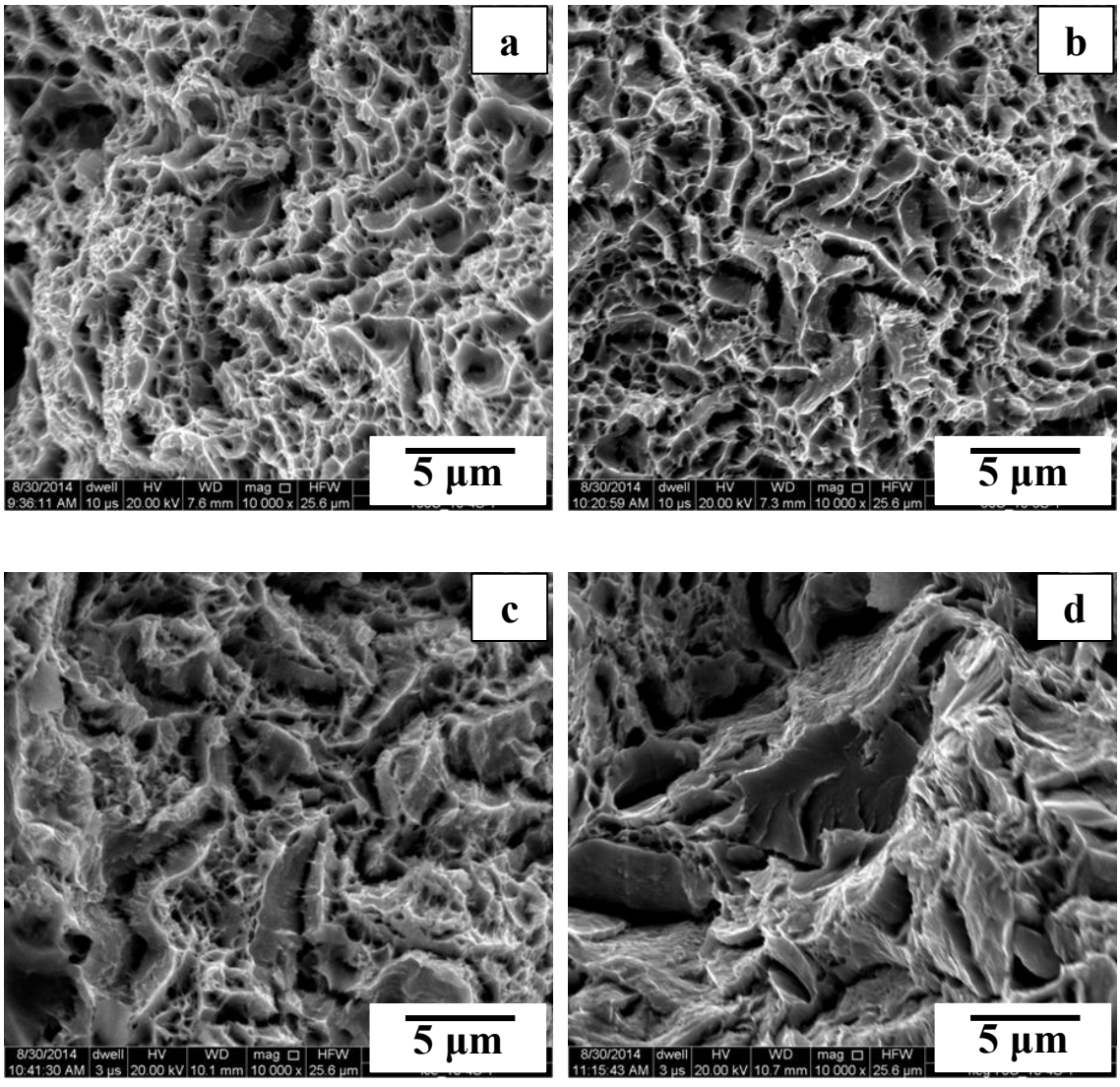

Fig. 4.3. Magnified view of central fibrous zones of the N_1+T specimens tested at different temperatures: (a) 100 °C (b) 80 °C, (c) 0 °C, & (d) -70 °C.

There is increase in the number and size of the facets, associated cracks, and decrease in number and size of the dimples with fall in test temperature (Fig. 4.3 b–d).

Surface morphology of the petal shaped segments was similar to those of their respective fibrous zones (Fig. 4.4).

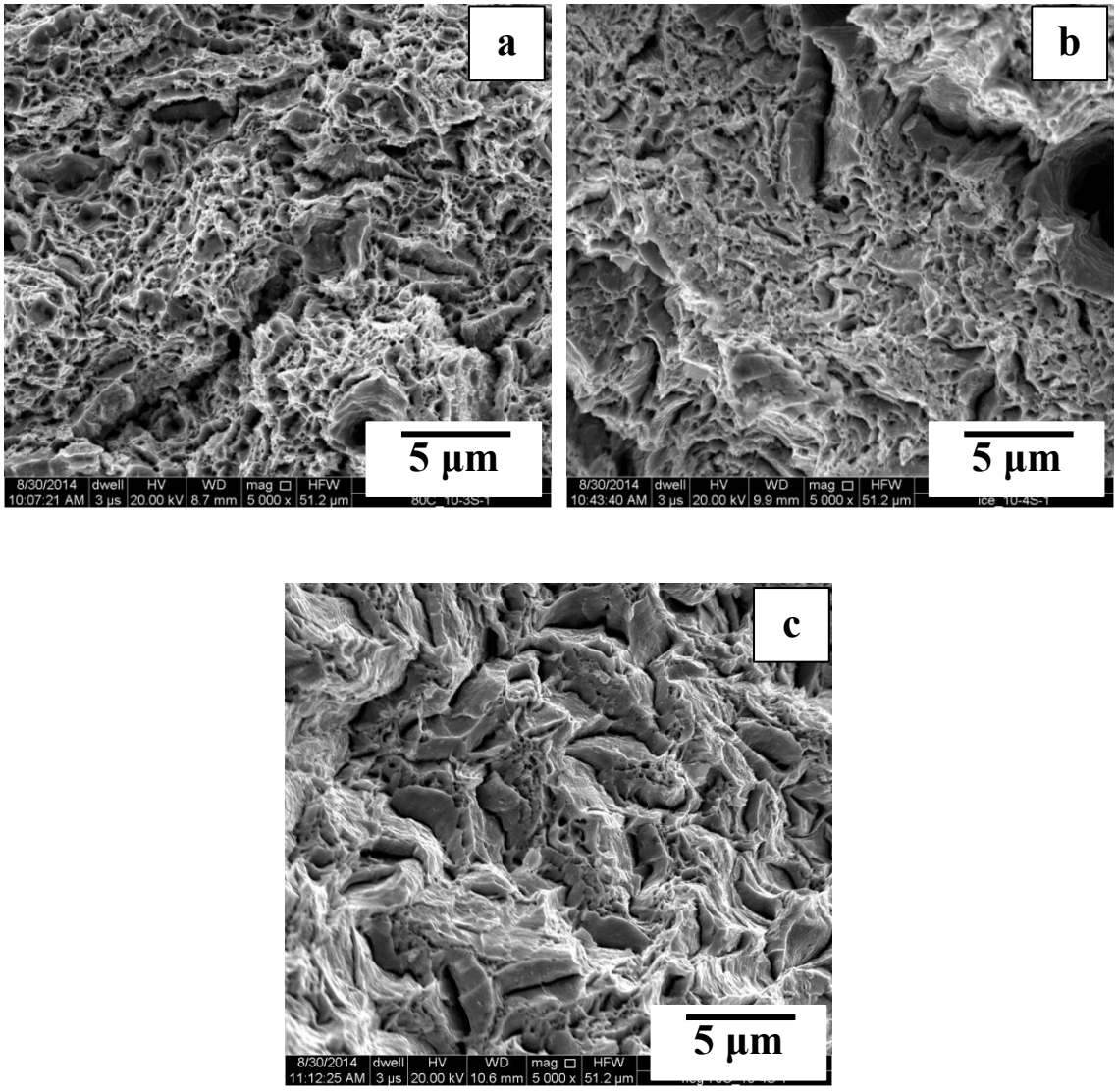

Fig. 4.4 Magnified view of petal shaped region of the N_1+T specimens tested at different temperatures: (a) 80 °C, (b) 0 °C, (c) -70 °C.

4.3 Effect of Specimen Orientation

In an earlier investigation longitudinal splitting was reported to occur along rolling texture of the material [108,109]. In order to examine the effect of texture on

fracture behavior, tensile tests were conducted for specimens oriented at different angles to the rolling direction. Tensile properties (YS, UTS & % elongation) are examined for the specimens oriented parallel to rolling direction, at 45° and 90 ° to the rolling direction as shown in Fig. 4.5. Both, the yield as well as tensile strength of the specimen oriented at 45 ° to the rolling direction is higher, however, its ductility is lower.

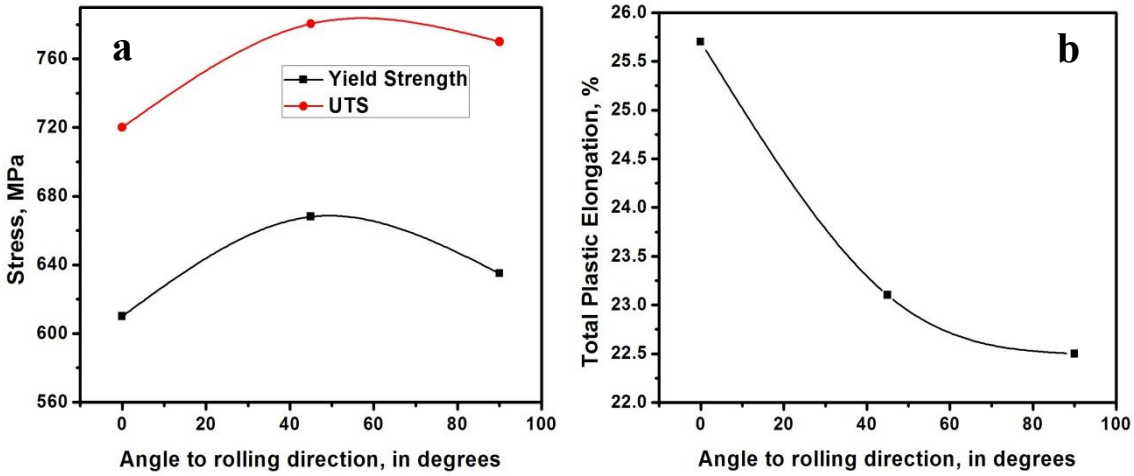

Fig. 4.5 Effect of specimen orientation with respect to rolling direction in the N_1+T condition on: (a) yield strength and ultimate tensile strength, (b) total elongation.

The morphology of fracture surfaces of the specimens oriented at 0 °, 45 ° & 90 ° with the rolling direction is shown in Fig. 4.6. It may be seen that there is longitudinal splitting in all the specimens, irrespective of their orientation with the rolling direction. Longitudinal splitting has been reported in warm–rolled steel in the specimen oriented parallel to rolling direction and has been attributed to texture effect [108]. However, it is obvious from the present investigation that occurrence of longitudinal splitting is independent of the orientation of the test specimen. Thus, longitudinal splitting is an inherent fracture characteristic of this steel in the normalized & tempered condition.

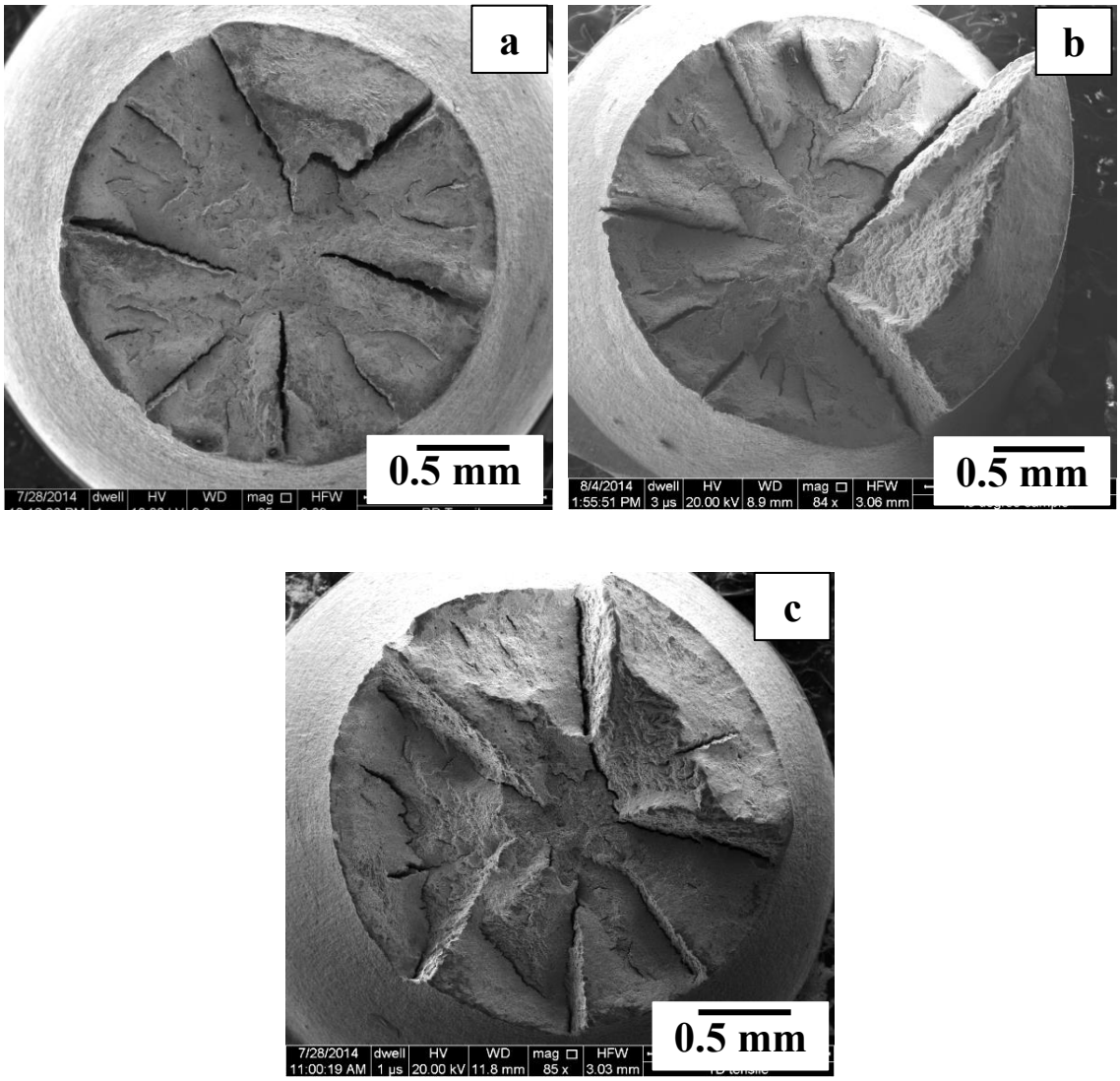

Fig. 4.6 Effect of the specimen orientation with respect to rolling direction on rosette fracture in the N_1+T condition: (a) along rolling direction, (b) at 45 ° to the rolling direction, (c) at 90 ° to the rolling direction.

4.4 Effect of Microstructure

Different heat treatments such as annealing, normalizing and quenching are given to study the impact of different resulting microstructures. The temperature and soaking time of heat treatment was increased in order to bring out the effect of different types of carbides on fracture behavior. All the heat treatments were given to the as supplied material which had already been normalized at 1060 °C for 1 h and tempered

at 780 °C for 1 h and is designated as N_1+T in this chapter. Details of the different heat treatments and their designations are given in Table 2.3 of chapter 2. Microstructures resulting from the above heat treatments are shown in Fig. 4.7. There was martensitic transformation in the A, N_2 & S_2+WQ specimens. In the N_2+T condition second phase particles reappeared and the number density as well as size of precipitates is larger in the N_2+T condition (Fig. 4.7c) as compared with that in the N_1+T and A condition (Fig. 4.7 a & b) and the quantitative values are given in table 4.1.

Table 4.1: Area fraction of carbides in different heat treated conditions.

Heat Treatment	A	N_1+T	N_2+T
Area Fraction (%)	6.12	12.37	36.59

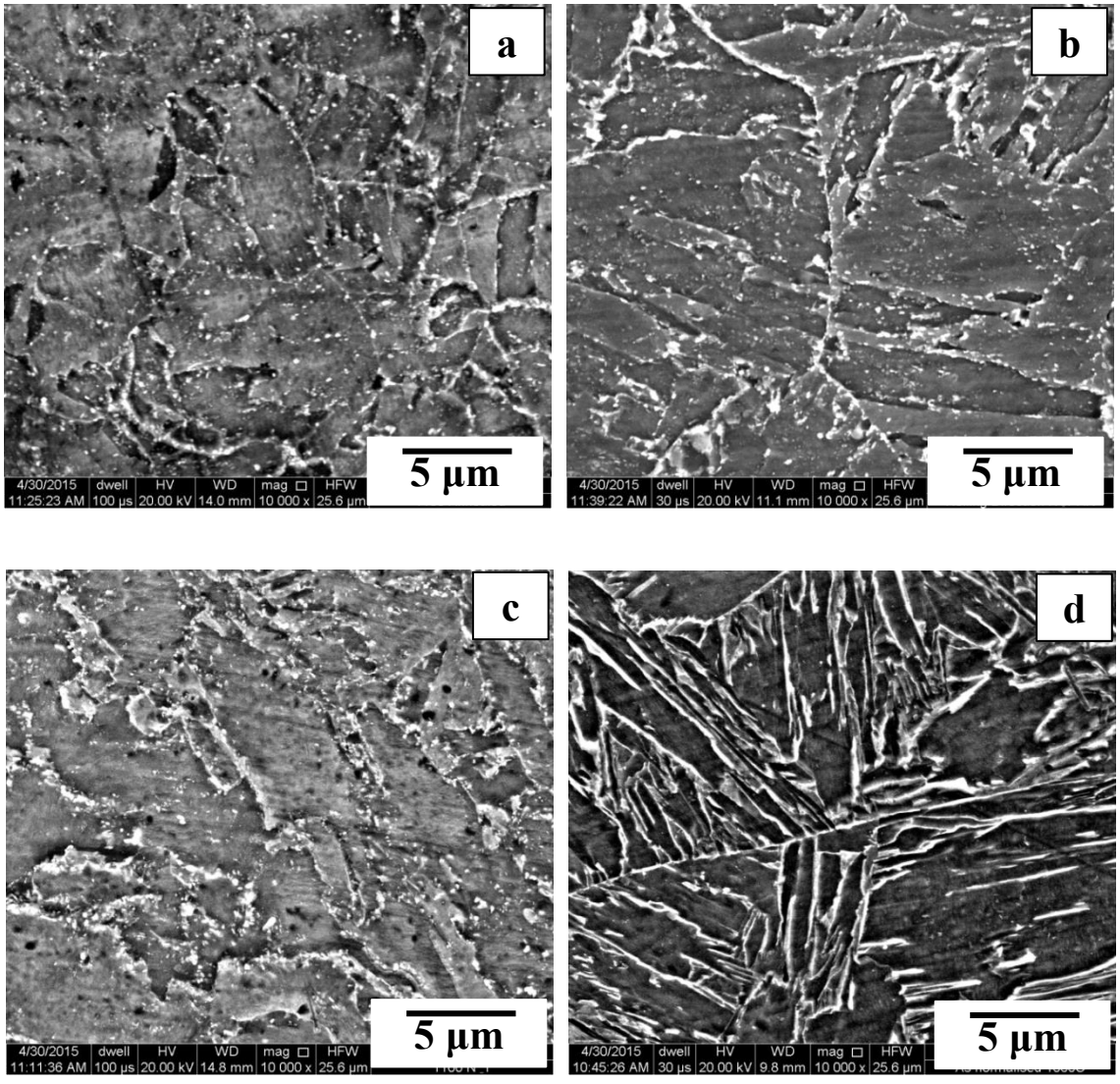

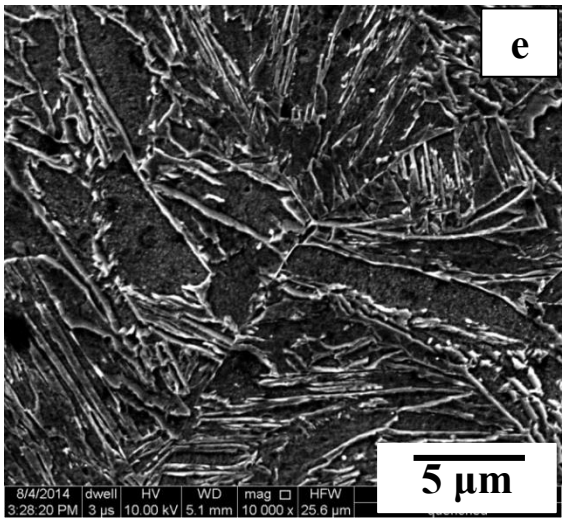

Fig. 4.7 SEM micrographs showing microstructures of the specimens in different heat treated conditions (a) A, (b) N_1+T (As received), (c) N_2+T, (d) N_2 & (e) S_2+WQ.

The overall fracture morphology of the different heat treated specimens, tested in tension, is shown in Fig. 4.8 (a–e). Radial cracking is not observed in the A, N_2 and S_2+WQ specimens as is evident from Fig. 4.8 (a–c). On the other hand, radial cracking is observed in the N_2+T specimen (Fig. 4.8d). Brittle fracture is observed in the S_2+WQ specimen and there is quasi–cleavage fracture in the A & N_2 specimens.

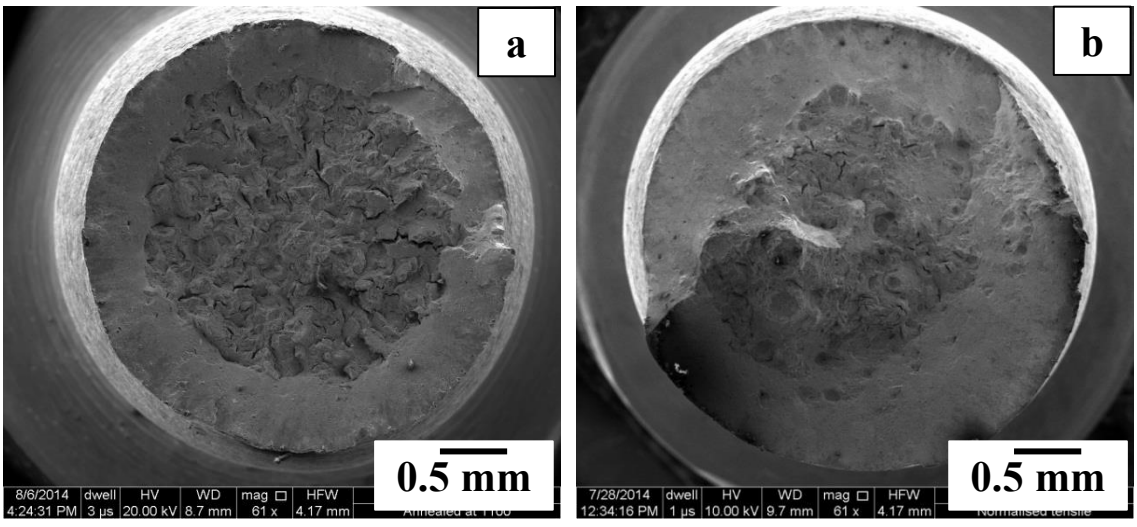

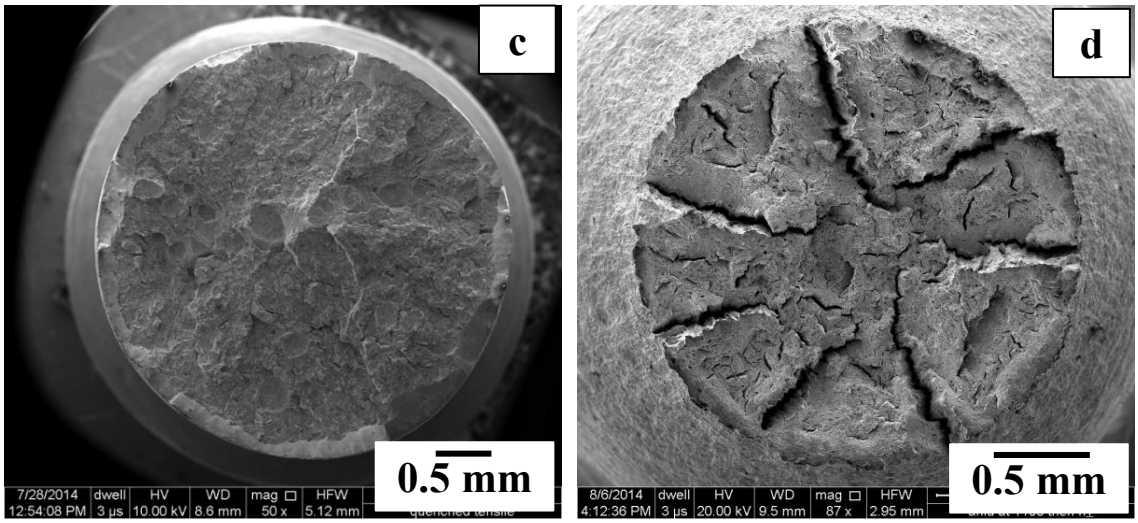

Fig. 4.8 Fracture surfaces of the specimens in different heat treated conditions: (a) A, (b) N_2, (c) S_2+WQ & (d) N_2+T.

4.5 Effect of Strain Rate

Tensile tests are conducted at different strain rates from 10^{-2} s^{-1} to 10^{-4} s^{-1} to examine the effect of strain rate on fracture behavior. Full views of fracture surfaces of round tensile specimens of N_1+T, tested at three different strain rates and are shown in Fig. 4.9. It is obvious that there is rosette fracture at all the strain rates. The number of radial cracks with longitudinal splitting was almost comparable and also the area of shear lip zone and fibrous zone is independent of strain rate.

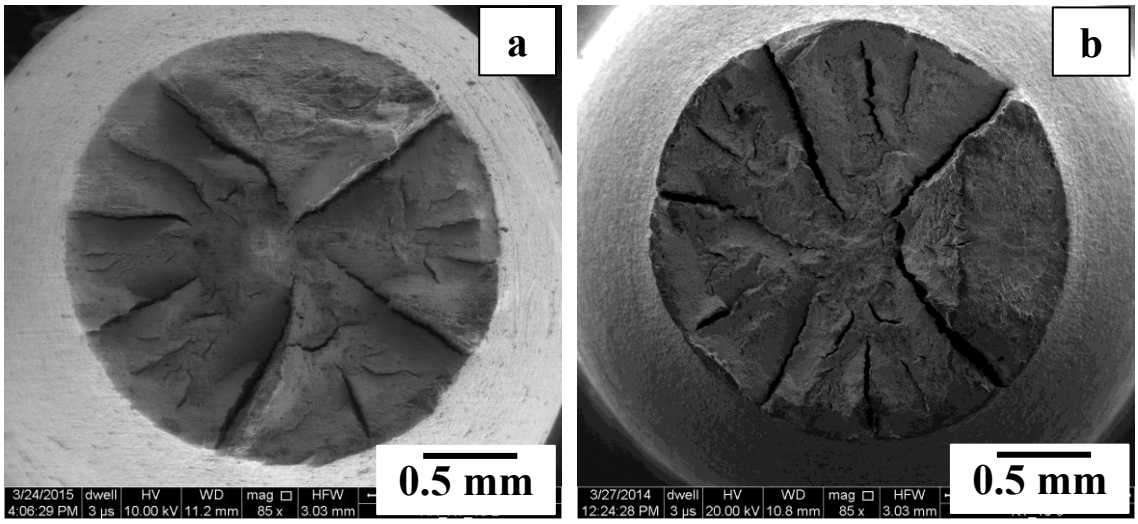

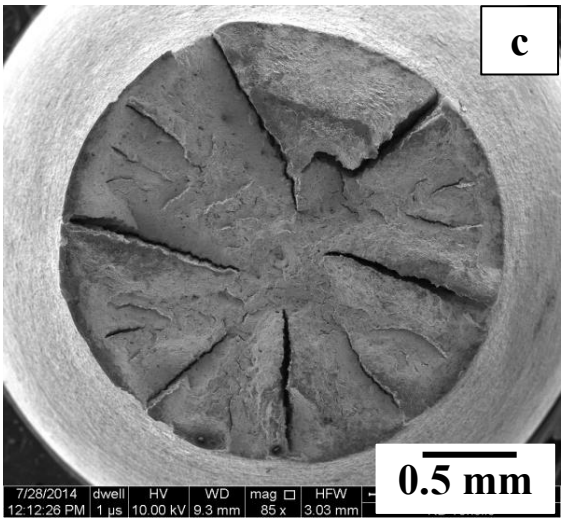

Fig. 4.9 Fracture surfaces of normalized and tempered specimens tested in tension at RT at three different strain rates: (a) 10^{-2} s^{-1}, (b) 10^{-3} s^{-1}, and 10^{-4} s^{-1}.

4.6 Effect of Specimen Size

It has already been mentioned that rosette fracture with longitudinal splitting was observed in round tensile specimen of 4.5 mm diameter at all the three strain rates referred to above. In order to understand the effect of size of tensile specimen on fracture behavior, tensile tests were conducted also for flat specimens of different thicknesses. The effect of thickness on fracture behavior is shown in Fig. 4.10. It is obvious from these fractographs that longitudinal splitting is affected by thickness of the specimens. Longitudinal splitting is negligible in the thin specimen of 1.75 mm thickness, however, its tendency increased with increase in thickness. As the thickness of the specimen increased from 1.75 mm to 4.5 mm, the tendency for longitudinal splitting also increased. Thus, it is worth mentioning that triaxiality is also essential for longitudinal splitting in tensile fracture. Triaxiality increases with increase in thickness of flat specimen [110].

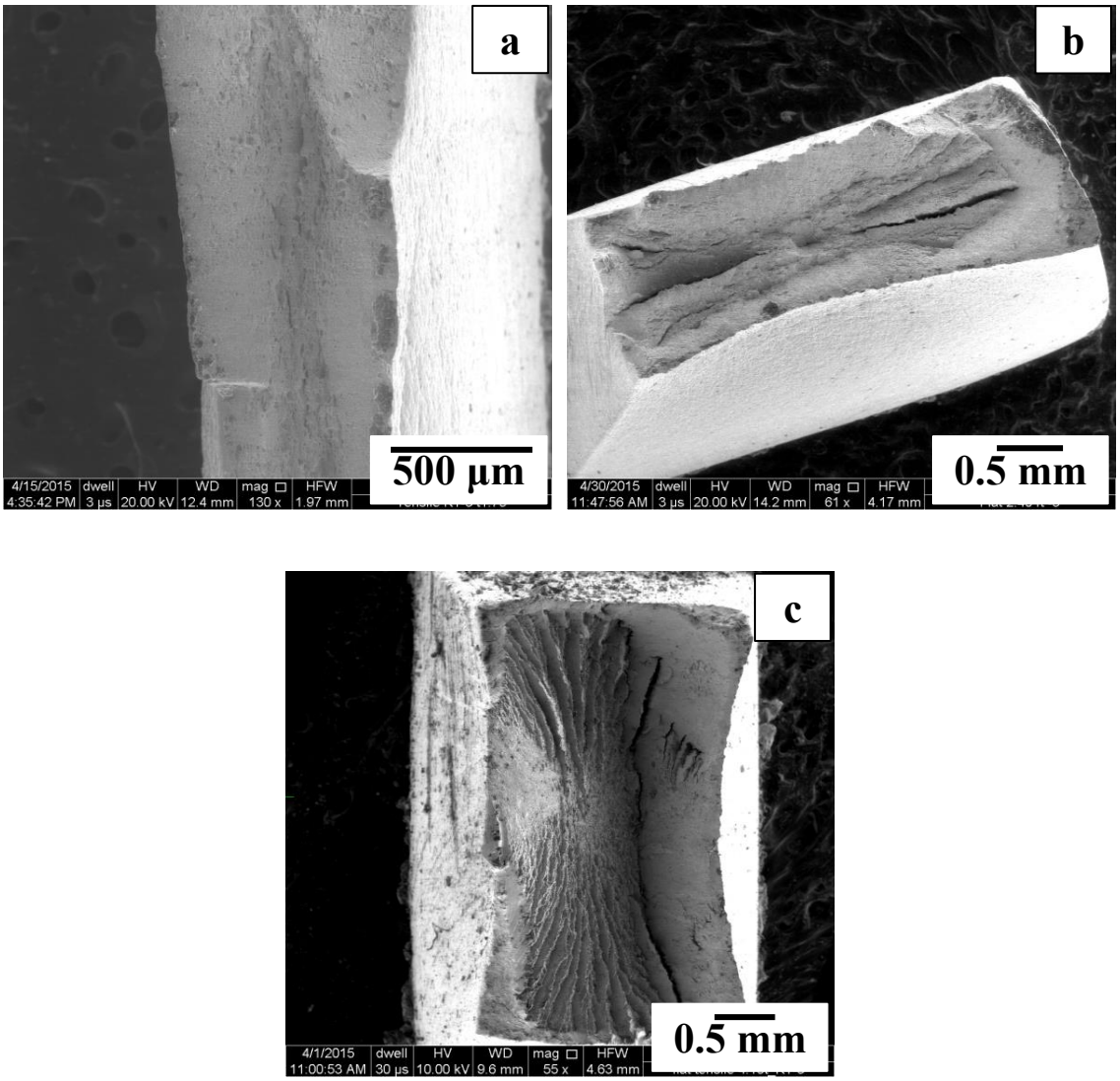

Fig. 4.10 Overall view of fracture surfaces of flat tensile specimens of different thicknesses: (a) 1.75 mm, (b) 2.4 mm, and (c) 4.5 mm.

4.7 Discussion

Different terminologies have been used for radial cracking/longitudinal splitting such as, rosette fracture, split fracture, delamination and star fracture. In view of the appearance of fracture surfaces in the present investigation, rosette fracture appears to be more appropriate.

The modified 9Cr–1Mo steel exhibits usual cup and cone fracture at 100 °C, however, with decrease in temperature there was long splitting parallel to tensile axis.

Disappearance of rosette fracture at 100 °C may be understood in terms of higher ductility of the material and relatively less deleterious effect of second phase particles on the fracture behavior. The ductile to brittle transition temperature (DBTT) for this steel has been reported -37 °C [111]. The ductility of this steel is found to be almost constant over the temperature range investigated. Delamination has been reported to improve toughness in a wide variety of materials; for example in ceramics [112], carbon [113] and fine–grained steels [114–116]. Delamination in low alloy steels occurs when the stress along normal direction (ND) of the plate exceeds a critical value which is lower than the critical cleavage stress along the rolling direction (RD) and the long transverse directions (TD). This difference is attributed to shape anisotropy of ferrite grains [117]. It may be seen from the SEM micrographs that there is precipitation of $M_{23}C_6$ and vanadium carbides along the prior austenite grain boundaries in condition A (Fig. 4.7a), N_1+T (Fig 4.7b), and N_2+T (Fig. 4.7c). Carbide particles may be seen also along the lath boundaries. While the number density of carbide particles is much higher in the N_1+T (Fig. 4.7b), and N_2+T (Fig. 4.7c) it is quite low in the A condition (Fig 4.7a). In contrast to the above three conditions, the number density as well as the size of carbide precipitates in N_2 (Fig. 4.7d) and S_2+WQ (Fig. 4.7e) condition is much less. Dissolution temperature of different precipitates is given in Table 4.2. Likewise, some small and discontinuous cracks occurred in the annealed material (Fig 4.8a). A few cracks of very fine size may be seen in N_2 condition (Fig. 4.8b) and no cracks in S_2+WQ condition (Fig. 4.8c). On the other hand, several large radial cracks and fine cracks may be seen in the flat petal shaped segments of the N_2+T specimen (Fig. 4.9d). There is relatively higher severity of radial cracking in N_2+T (Fig. 4.9d) than that in N_1+T condition (Fig. 4.2e).

Table 4.2: Dissolution temperature of different type of carbides.

Carbides	$M_{23}C_6$	VC	NbC	Reference
Dissolution Temperature	870 °C	1080 °C	1150 °C	*Shreshtha et al. Metals* **2015**, *5*, 131

Occurrence of nearly comparable rosette fracture in the specimens oriented at 0°, 45 ° and 90 ° to the rolling direction suggests that rosette fracture in the modified 9Cr–1Mo steel is independent of the orientation of the test specimen. This corroborates with macrotexture of this steel that is found to be random. Rosette fracture in the modified 9Cr–1Mo steel is found to be strongly affected by the heat treatment. In order to understand the effect of heat treatment on fracture behavior of this steel, bulk texture is analyzed for the different heat treated conditions. Orientation distribution function (ODF) corresponding to 45 ° for Bunge angle is shown in Fig. 4.11 for the different heat treated conditions. It is obvious from the ODF figures that there is strong γ–fibre in the N_1+T in comparison with that in A condition (Fig. 4.11 a–b). Presence of γ–fibre is known to be the signature of good ductility. Higher ductility exhibited in N_1+T than that in A condition may thus be understood. Intensity of cube texture is high in the N_2 (Fig. 4.11c) and in S_2+WQ (Fig. 4.11d) in comparison with that in the S_2+WQ+T (Fig. 4.11e). γ–fibre components are strong in the S_2+WQ+T condition (Fig. 4.11e). Development of strong γ–fibre texture offers higher strength and better impact toughness. On the other hand, presence of Goss texture and rotated cube texture would have a negative effect on impact toughness of this steel [111]. Thus, it may be seen that variation in the texture component affects mainly the mechanical properties like strength and ductility in the different heat treated conditions but not the fracture behavior.

Also a comparable value of texture index in the different heat treated conditions (N_2: 1.104, S_2+WQ: 1.096, & S_2+WQ+T: 1.138) indicates random texture in all the conditions. It may thus be inferred that rosette fracture with longitudinal splitting observed in the modified 9Cr–1Mo steel is independent of texture.

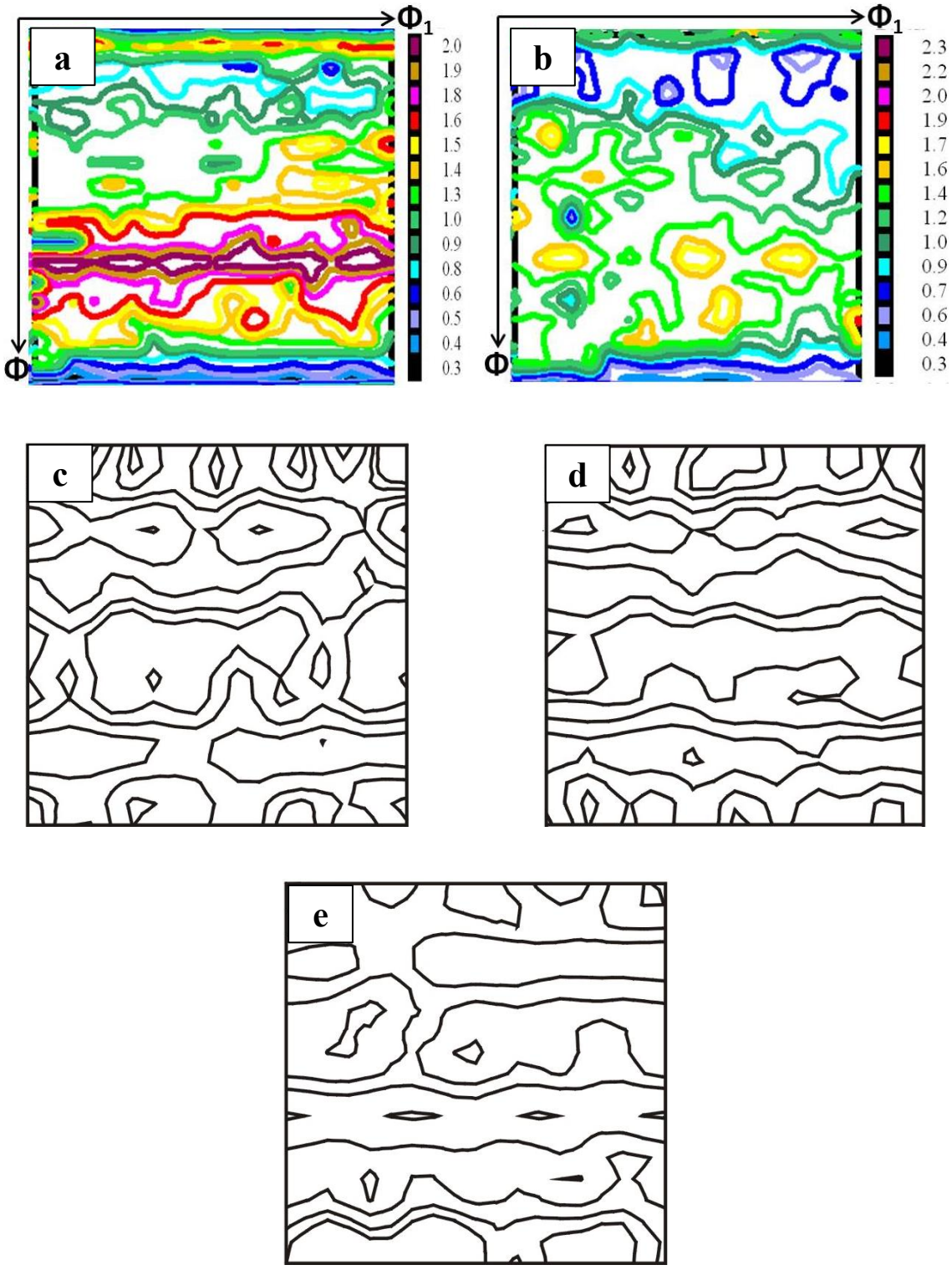

Fig. 4.11 Orientation distribution function (ODF) corresponding to ϕ_2 = 45° section as obtained from the macrotexture examination of different heat treated specimens: (a) N_1+T, (b) A, (c) N_2, (d) S_2+WQ, and (e) S_2+WQ+T.

Several investigators [118–120] have related rosette fracture in low carbon steels to distribution and morphology of carbides, or to cleavage along (100) planes [121–123]. Splitting has been reported to mechanical fibering (alignment of impurity, inclusions or voids) [124]. Delamination or longitudinal splitting has been reported also in other materials like AXI pipeline steel and low alloy steels and in all these materials it occurred in the range of ductile brittle transition temperature. Bramfitt et al. [125] observed delamination in low carbon steel and attributed to decohesion of grain boundaries, independent of texture of the material, and splitting was found to increase with decrease in finish temperature.

Tensile tests were interrupted for N_1+T specimens at maximum load (11 kN) and in the region of necking at 9 kN and 7 kN loads prior to fracture at the load of 6 kN to understand the process of rosette fracture. Longitudinal sections of the interrupted specimens were examined under SEM and are shown in Fig. 4.12. There was neither void formation in the vicinity of precipitates nor longitudinal cracking in longitudinal section of the specimen interrupted at the maximum load (Fig. 4.12a). However, further deformation in the region of necking caused void formation at second phase particles associated with grain boundaries/lath boundaries (Fig. 4.12b) due to triaxial state of stress resulting from addition of tangential stress along periphery of the fibrous zone (penny shaped crack) and radial stress from necking. The linkage of voids along the prior austenite grain boundary may be clearly seen from the fractured specimen (Fig. 4.12e).

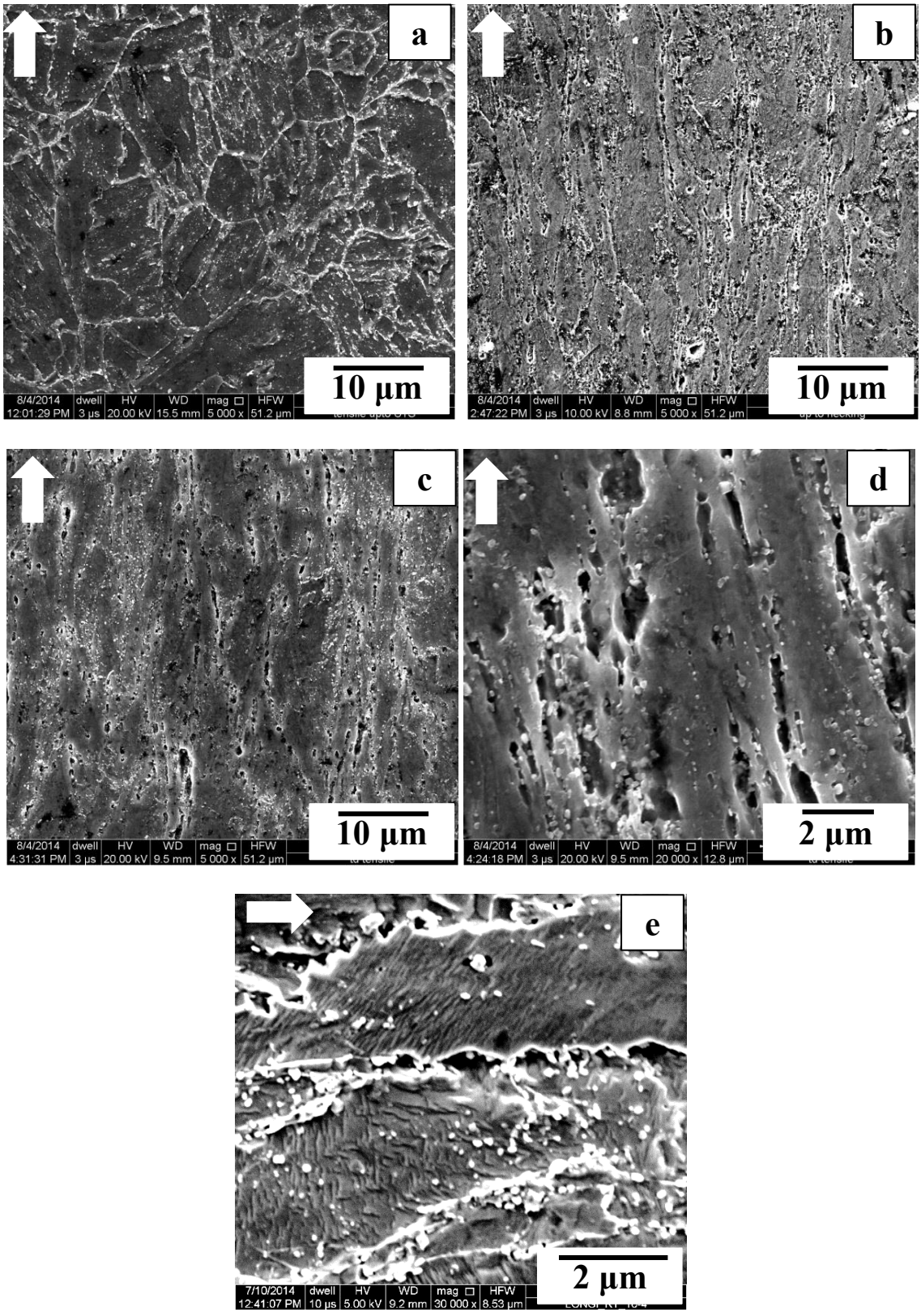

Fig. 4.12 Longitudinal sections of tensile specimens of N1+T, interrupted at different stages of deformation: (a) at maximum tensile load of 11 kN, (b) in necked region at 7 kN load, (c) fractured specimen at 6 kN load, (d) magnified view of (c), (e) showing linkage of voids along prior austenite grain boundaries. Tensile axis direction is shown by arrow.

It may be noted that there is pronounced tendency of longitudinal splitting resulting from preferred linkage of elliptical voids along the loading axis due to continued increase in major axes of the elongating elliptical voids and consequent decrease in the gap between the ends of adjacent elliptical voids. On the other hand, linkage of the elliptical voids associated with transverse grain/lath boundaries was delayed because of increasing separation between the adjacent voids due to continued decrease in minor axes of the associated elliptical voids and consequent increase in distance between them. The magnitude of the axial tensile stress increases with progressive necking. The tangential stress associated with periphery of the penny shaped crack promotes splitting of the longitudinal cracks in opening mode, at 90° to the stress axis causing fracture. In order to examine the features of fracture at longitudinal surface, the fractured specimen was broken along the split lines. It was done by drilling out the fibrous zone longitudinally and sectioning the drilled length of 0.5 mm from the fractured end transversely, with a slow speed cutter and all small pieces were separated.

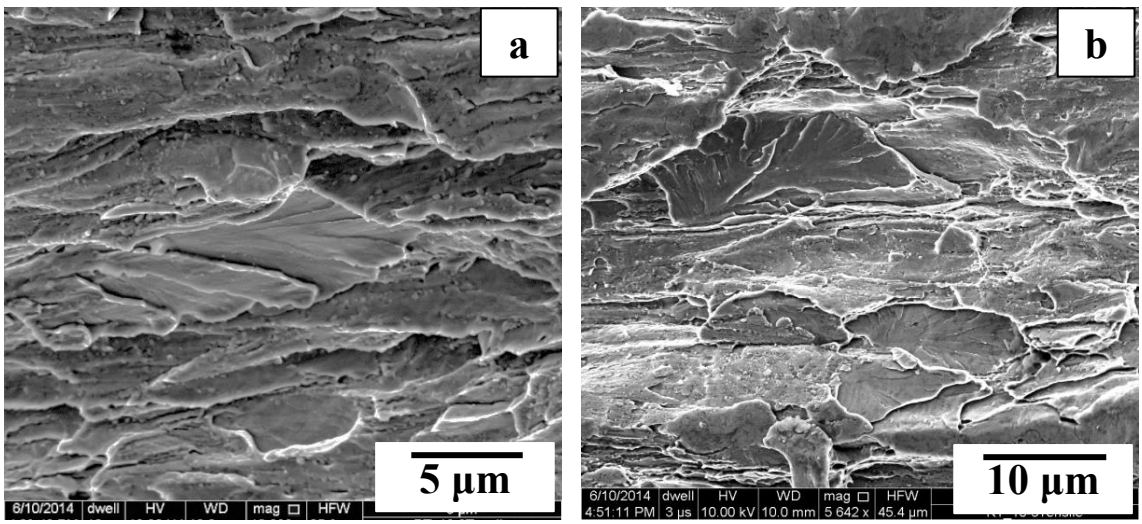

Fig. 4.13 Cleavage fracture resulting from longitudinal splitting of N_1+T specimen tested in tension.

Longitudinal surface were examined under SEM. There are large facets with river patterns characterizing cleavage fracture on the longitudinal split surface (Fig. 4.13).

Reduction in ductility with increase in volume fraction of second phase particles may be attributed to reduction in plastic strain because of rapid growth and linkage of voids formed. When the particle size was large, interaction took place in beginning of the plastic deformation [126]. In this steel, density of second phase particles along the prior austenite grain boundaries was high. Longitudinal section of the as annealed specimen tested at RT till fracture was also examined; however, no cracks were observed along the prior austenite grain boundaries parallel to the loading direction (Fig.4.14a). Longitudinal sections of the N_2 and S_2+WQ specimens also did not show any void (Fig.4.14 b & c). The {100} plane is a cleavage plane in iron, so the brittle cracks mainly propagate along the {100} plane.

Formation of neck introduces a triaxial state of stress, adding the tangential and radial stresses that act on the planes and facilitate the rosette fracture [127]. In case of BIS 812 EMA and the Q1N parent plate steels, the condition for star fracture and longitudinal splitting appears to be extensive plastic deformation producing alignment of voids nucleating at particles, low temperatures, and a triaxial state of stress resulting from enhanced tangential and radial stresses [128].

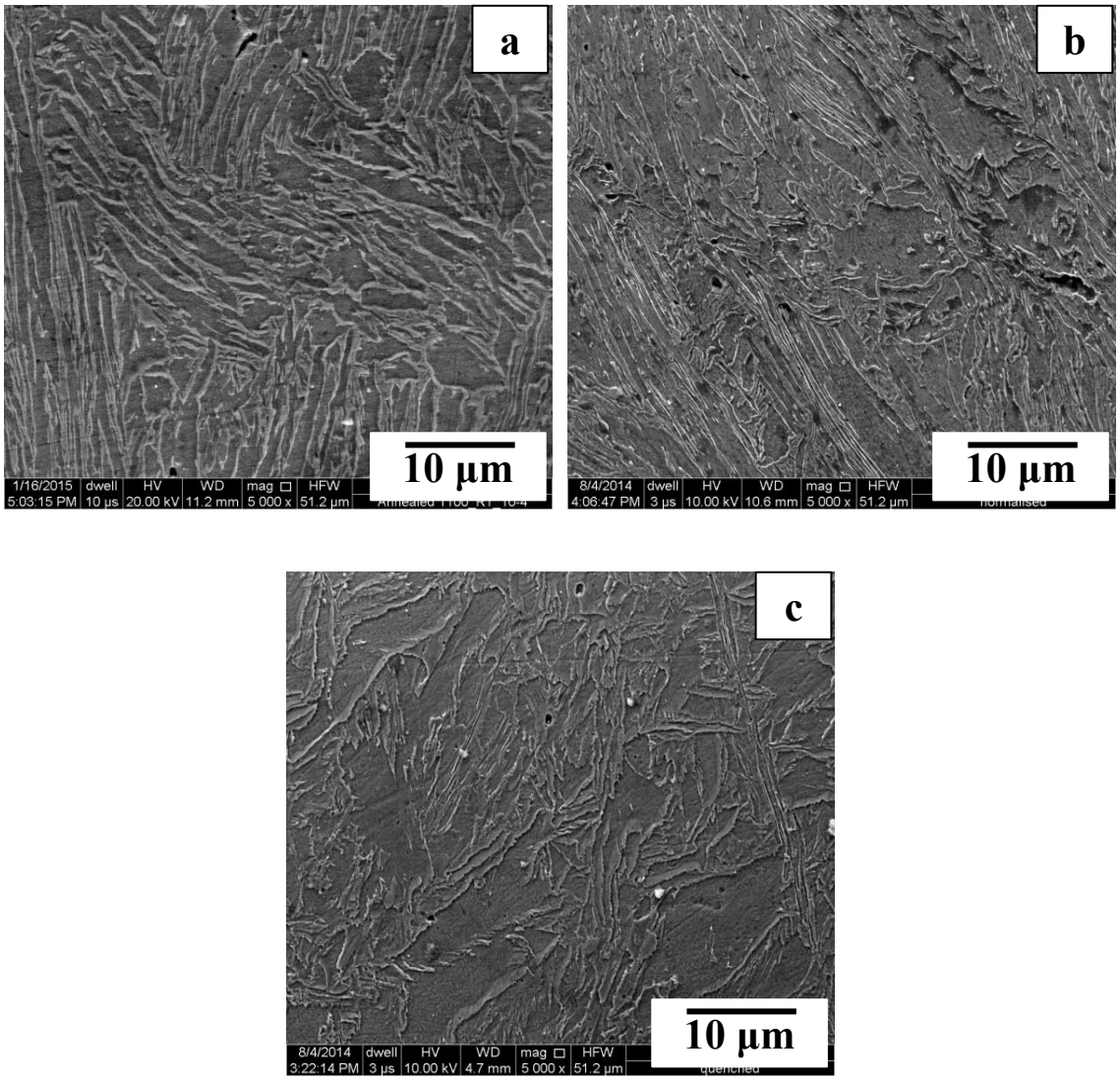

Fig. 4.14 Longitudinal sections of the fractured tensile specimens of different heat treated specimens: (a) A, (b) N_2, (c) S2+WQ.

Effect of triaxiality on rosette fracture was examined by testing flat specimens of different thicknesses. Effect of specimen thickness on longitudinal splitting is shown in Fig. 4.10. Longitudinal splitting is found to be reduced with decrease in specimen thickness. This may be understood in terms of the overall out of plane constraint and increase in the size of high constraint with increase in thickness [110]. It is well known that constraint to plastic deformation is maximized in thick specimens under plane strain

condition so that the energy absorbed during fracture is reduced as compared with that in thin specimen subjected to plane stress condition [110].

Longitudinal splitting during fracture reduces the out–of–plane constraint and enhances the tendency for ductile fracture. Longitudinal splitting and star fracture occur because of high ductility where large hoop and radial stresses develop within the neck of the tensile specimen and the high level of plastic deformation which creates region of low toughness within the necked region [127]. This is enhanced by formation of neck and by creation of longitudinal regions of reduced fracture toughness. It may be seen from the variation of mechanical properties with test temperature (Fig. 4.1) that the effect of temperature on ductility is marginal where rosette fracture was observed. Thus, longitudinal splitting does not cause any deterioration of ductility. This is consistent with the earlier observation [129].

A possible mechanism based on the microstructural observation for longitudinal splitting in tensile fracture is shown schematically in Fig. 4.15. The initial microstructure of the steel before loading, consists of second phase particles distributed along the prior austenite grain boundaries, lath boundaries and within the laths (Fig. 4.15a). Voids form around the second phase particles and get elongated in the direction of stress axis, in the region of necking (Fig. 4.15b). The distance between the initially formed spherical voids, along the longitudinal grain boundary is Y, and along the transverse boundary is X, and both are approximately equal. However, these distances would change with further deformation. It is quite obvious that the distance between the tips of the aligned elliptical voids is reduced from Y to Y' along the longitudinal boundary, whereas the distance between the parallel elliptical voids along the transverse boundary is increased from X to X' (Fig. 4.15c). Thus, easy linkage of voids along the grain boundary/lath boundary aligned parallel to stress axis gives rise to

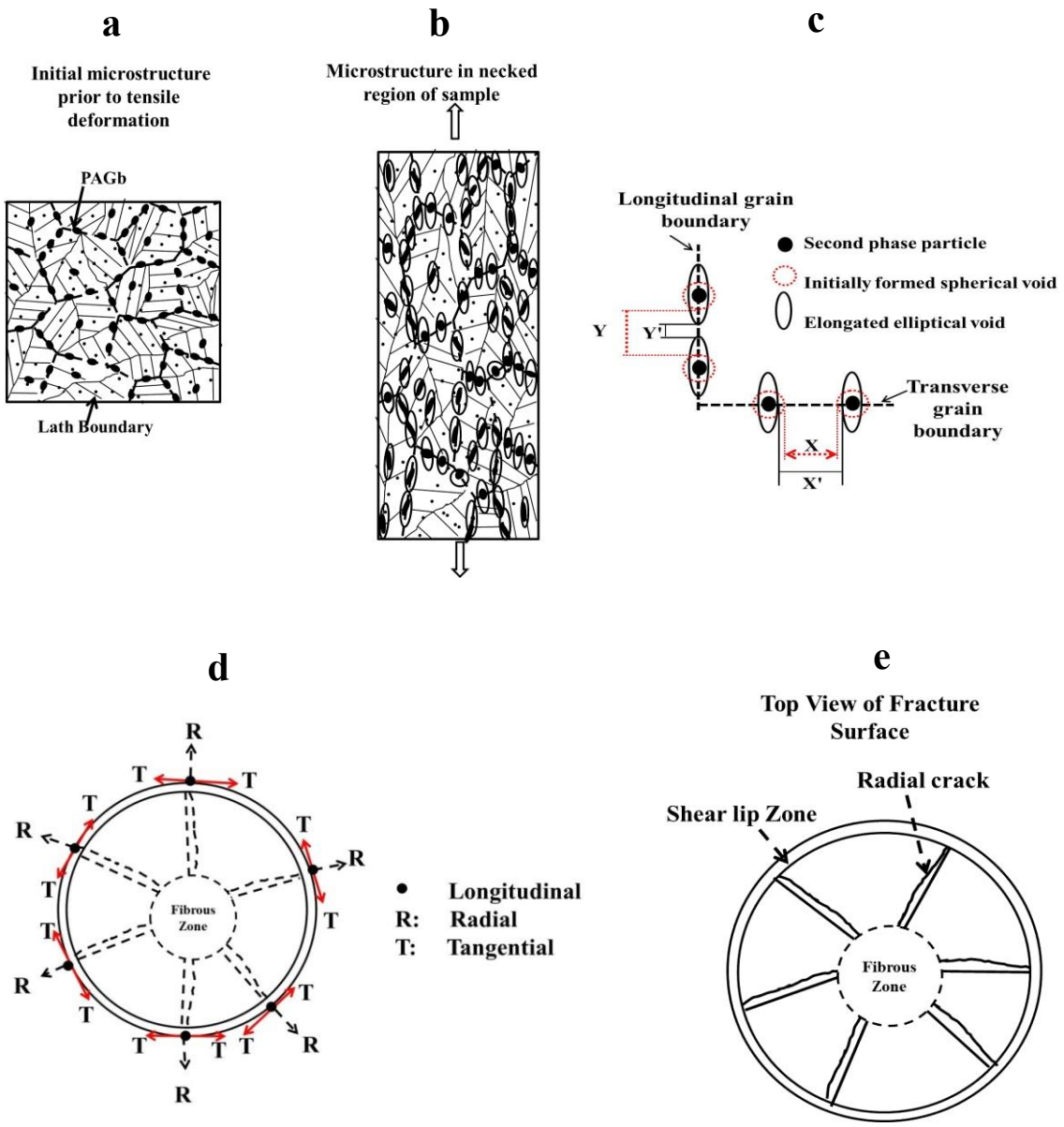

Fig. 4.15 Schematic of rosette fracture in N_1+T condition of the modified 9Cr–1Mo steel at RT (a) initial microstructure in unloaded condition, (b) voids formed at second phase particles on tensile loading in the region of necking, (c) easy linkage of voids lying along longitudinal grain boundaries, (d) triaxial stresses acting in the necked region of the specimen, & (e) rosette fracture.

the so called longitudinal splitting. Different stresses (longitudinal, radial and tangential) act in the necked region (Fig. 4.15d). The tangential stresses acting along the periphery of the penny shaped crack in the fibrous zone promote the tendency of spitting of the cracked longitudinal grain boundaries to result in cleavage fracture. Thus,

splitting of the longitudinal boundaries in different regions gives rise to the observed rosette fracture with petal shaped segments (Fig. 4.15e).

4.8 Conclusions

The following conclusions are drawn from this chapter:

- The modified 9Cr–1Mo steel exhibits rosette fracture with longitudinal splitting in the temperature range from -70 to 80 °C in tensile testing and the severity of longitudinal splitting increases with decrease in temperature.
- Rosette fracture is independent of strain rate. It occurred due to alignment of void nucleating particles along prior austenite grain boundaries and lath boundaries oriented along the stress axis under the triaxial state of stress during necking.
- Rosette fracture in tensile testing is affected by microstructure, in particular the precipitation of carbides.
- There is no effect of texture on rosette fracture resulting in this steel from tensile test.